Updated track fitting and alignment method for the silicon tracking telescope at the Fermilab Test Beam Facility

Kelly Stifter

University of Minnesota
Minneapolis, MN 55455

Science Undergraduate Laboratory Internship

Scientific Computing Division
Fermi National Accelerator Laboratory
Batavia, IL 60510

(Dated: 8 August 2014)

The silicon tracking telescope at the Fermilab Test Beam Facility (FTBF), located at Fermi National Accelerator Laboratory, provides precise track fitting information to users wishing to test irradiated devices. In order to improve the track fitting process, an updated track fitting method for the telescope has been implemented. The update is based on a Kalman filter to improve the handling of errors in the track fitting process and account for the probability of multiple scattering off device material. Improved track fitting can translate to more accurate alignment of the device in addition to improved resolution for the user. The resolution and error handling of the updated method is compared to the original χ^2 minimization fit method. It is found that when the scattering probability is introduced into the Kalman filter, both the residuals and pull values for most detectors move away from the desired values. Despite that, the Kalman filter, assuming no multiple scattering, improves residuals and pulls for most detectors. For this reason, the Kalman filter will replace the standard track-fitting method in future analyses, though further study is needed in order to account for the probability of scattering.

CONTENTS

I. INTRODUCTION

A silicon pixel tracking telescope was originally developed at Fermilab in 2009 in order to provide precise particle tracking information to experiments at the MTEST beamline at FTBF.[1] It was comprised of eight planes of PSI46.v2 read out chips (ROCs) left over from the CMS forward pixel detector production. Four pixel planes are made of six ROCs laid out in a 2x3 grid and four are made of eight of the same ROCs laid out in a 2x4 grid. Each ROC is 80x52 pixels. The individual pixels have dimensions of 100x150 μm^2. When hit by a charged particle, the ROCs read out the pixel that has been hit, as well as the amount of charge deposited. From this information, the x- and y-coordinates of the hit can be determined. A 2x4 module is shown in Figure 1.

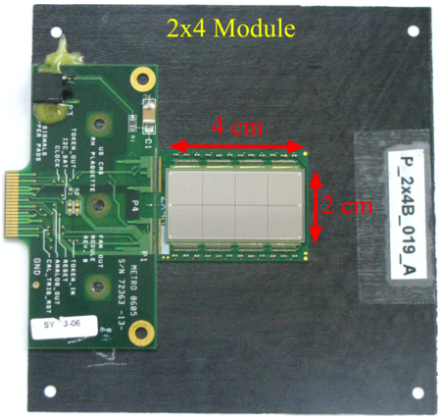

FIG. 1. PSI46.v2 Read Out Chips (ROCs) left over from the CMS Forward Pixel detector production are used in the pixel telescope. A 2x4 module is shown.

For global positioning, the $+z$, or downstream, direction is taken to be along the beam and $+y$ is taken as up, leaving $+x$ to be determined by the right-hand rule.

The eight pixel planes are placed in two stations of four detectors, one on either side of a center section, which is left open for the device under test (DUT). In each station, there are two 2x3 modules and two 2x4 modules. The downstream station is referred to as station 0, and the upstream station is referred to as station 2. The pixel planes are tilted around the smaller, 100 μm, dimension of the pixels so that the protons will often deposit charge in more than one pixel. Hits of this nature produce a better measurement of the location of the hit. Figure 2 gives a three-dimensional view of how the eight pixel planes are aligned in space.

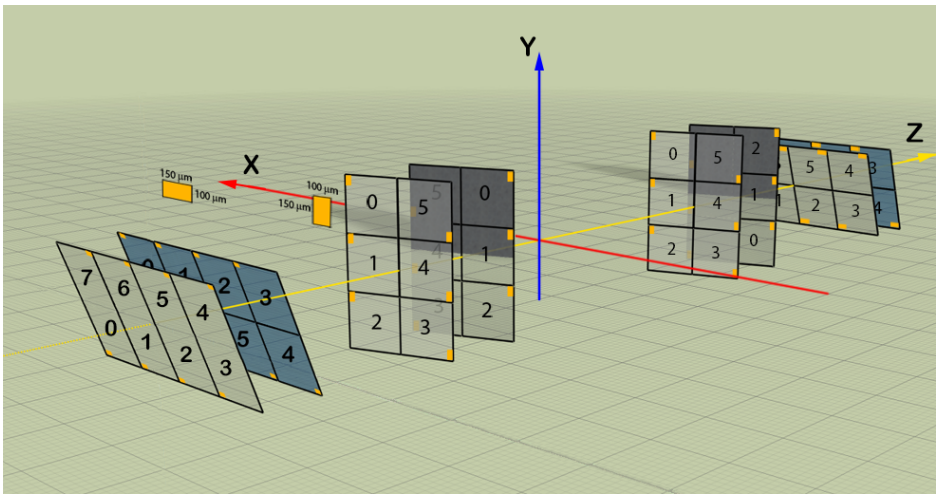

FIG. 2. A three-dimensional view of how the pixel planes are arranged in space.

In April 2014, the telescope was upgraded to include fourteen Hamamatsu silicon strip sensors made for the Run IIb D0 Layer 1 silicon detector.[2] The new strip telescope was built because the facility needed a larger area to cover devices and track particles. Each strip detector is 9 cm long and has 639 strips across with an individual strip width of 60 μm, for a total width of almost 4 cm. An example is shown in Figure 3. The strips are placed perpendicularly in groups of two, giving an overlap area of approximately 4x4 cm^2, as shown in Figure 4. The first strip in a pair is oriented to measure the x-coordinate, while the second is oriented to measure the y-coordinate. Both strips still read out the charge deposited.

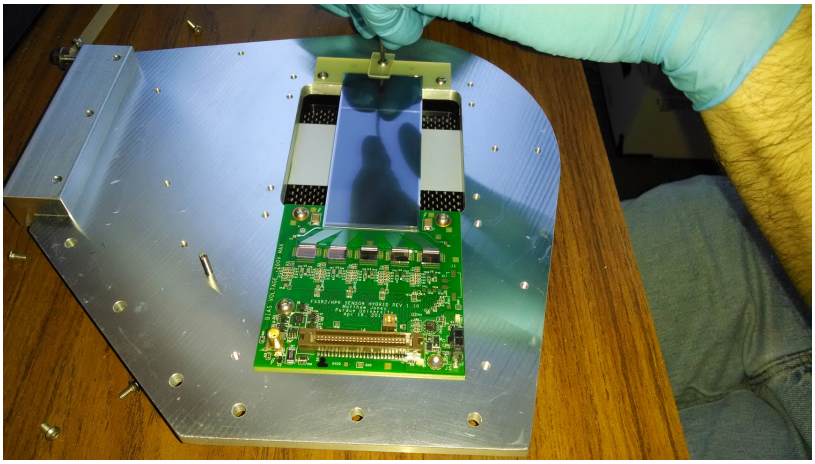

FIG. 3. Hamamatsu silicon strip sensors made for the Run IIb D0 Layer 1 silicon detector are used in the strip telescope.

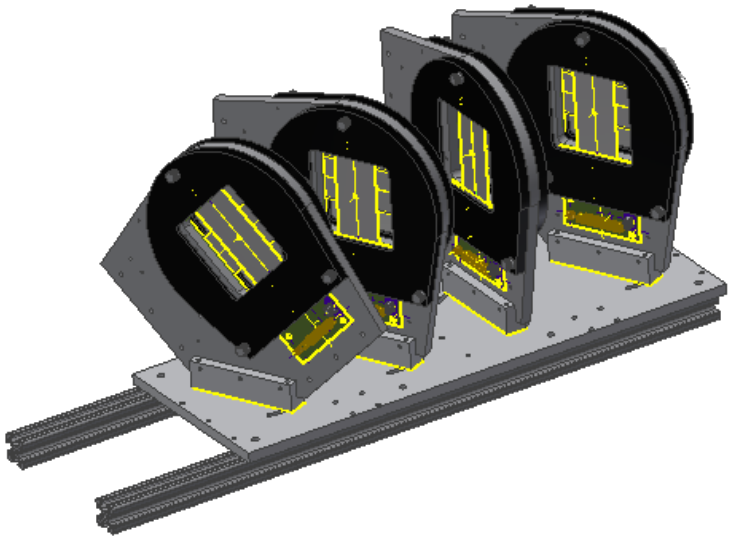

FIG. 4. Eight strips are shown in four pairs of two. Strips in pairs are placed orthogonally to one another in order to measure both x- and y-coordinates. While the strips can be tilted at 45°, as shown in the first pair, no pairs are currently tilted in this manner.

The fourteen strips are placed in three stations, two of four detectors and one of six. The strips are tilted around the y-axis by 15° so that the protons will often deposit charge in more than one strip. Again, this improves the ability to measure the location of the hit.

The two stations of four strips (referred to as stations 5 and 6) are placed upstream of the DUT and station 2, while the single station of six is placed downstream of the DUT and station 0. The whole device is approximately two meters long. An incomplete schematic of the device can be seen in Figure 5(a), and a downstream view of physical device can be seen in Figure 5(b). A scintillator located between station 0 and station 7 helps trigger events.

The MTEST beamline provides 120 GeV protons for four seconds every minute. The particles arrive 18 ns apart due to the 54 MHz accelerator clock. The detectors run at half that frequency, so data can be recorded every 36 ns. When the pixel telescope receives a trigger from a coincidence between the scintillator in the telescope and two other scintillators in the beamline, the pixel modules send data to the DAQs corresponding to the correct clock cycle. The strip planes are data-driven, so every hit above threshold is immediately read out. The hits are grouped into events using a timestamp coming from a counter incremented by the accelerator clock. The events are analyzed and the protons tracked through the telescope planes to determine where the hits should be located on the DUT.

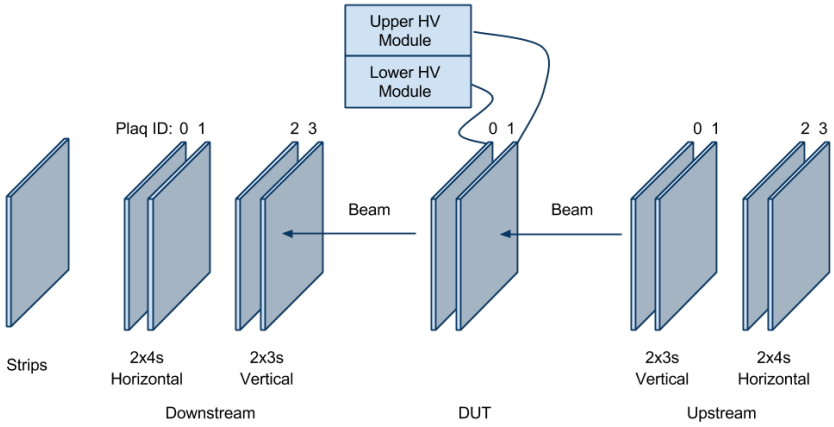

(a) Incomplete schematic of silicon tracking telescope

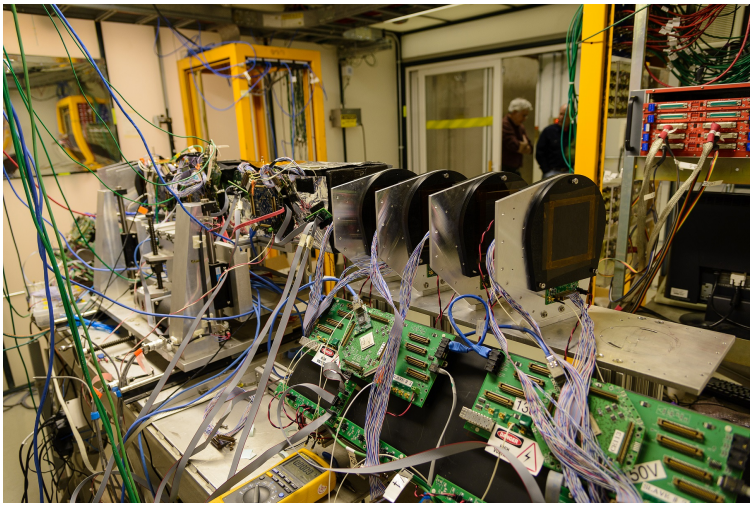

(b) Silicon tracking telescope at FTBF

FIG. 5. *Top:* A mock-up of the telescope as of November 2013. Currently, there are planes of strips on both the up- and downstream sides of the DUT. *Bottom:* The telescope in the MTEST beamline at FTBF. Planes of strips can be seen in the foreground.

The main role of the telescope is to test possible pixel candidates for the upcoming High Luminosity Large Hadron Collider (HL-LHC) upgrade. After the phase II upgrade, detectors at the LHC are expected to see an integrated luminosity of around 3000 fb^{-1}, which is about ten times higher than the detectors in the original LHC were designed to handle.[3] When silicon detectors are exposed to high amounts of radiation over long periods of time, their silicon lattice begins to degrade which causes a decrease in efficiency. Therefore, it is

necessary to understand the behaviors of new detectors under the heightened conditions of the HL-LHC before they are installed. Users wishing to test their new detectors have access to this high-precision, silicon tracking telescope to aid them in this task.

II. CURRENT METHODS

A. Track selection and fitting

Track fitting is a major component of the telescope, since the purpose of the device is to allow users to track protons through all of the planes in order to provide a precise hit location on the DUT.

Before there is even a track to fit, a few initial steps must be taken to analyze the raw data, executed in a software package called Monicelli.[4] Each event is processed, and all the hits on each plane are located. Hits that are next to each other are grouped together into a cluster. The program considers clusters composed of only one or two hits. The errors on clusters of different sizes are treated separately.

Once all of the hits in an event are located, they are searched for potential tracks. Monicelli takes user inputs, such as the minimum number of points per tracks and maximum number of tracks per event, and then searches the hits for potential tracks. To do so, the most upstream and most downstream hits are located and a line is drawn between them. Monicelli then searches along that line, within a user-specified tolerance range, for other hits. If more than the minimum amount of hits is found, it calls that collection of points a track. All of the tracks passing the final cuts are fit using a simple χ^2 minimization method.

B. Alignment

At the beginning of the track fitting procedure, the user inputs an initial geometry which they believe describes how the planes are laid out in space. Once all of the tracks are examined, graphs showing the beam spots on the detectors, as in Figure 6, are obtained. They show that the beam of protons has a distribution that is approximately Gaussian as it hits the detectors, but that the peaks are not lined up, which indicates that the mechanical alignment is not perfect.

It is impossible to physically measure this geometry with the μm resolution that is desired,

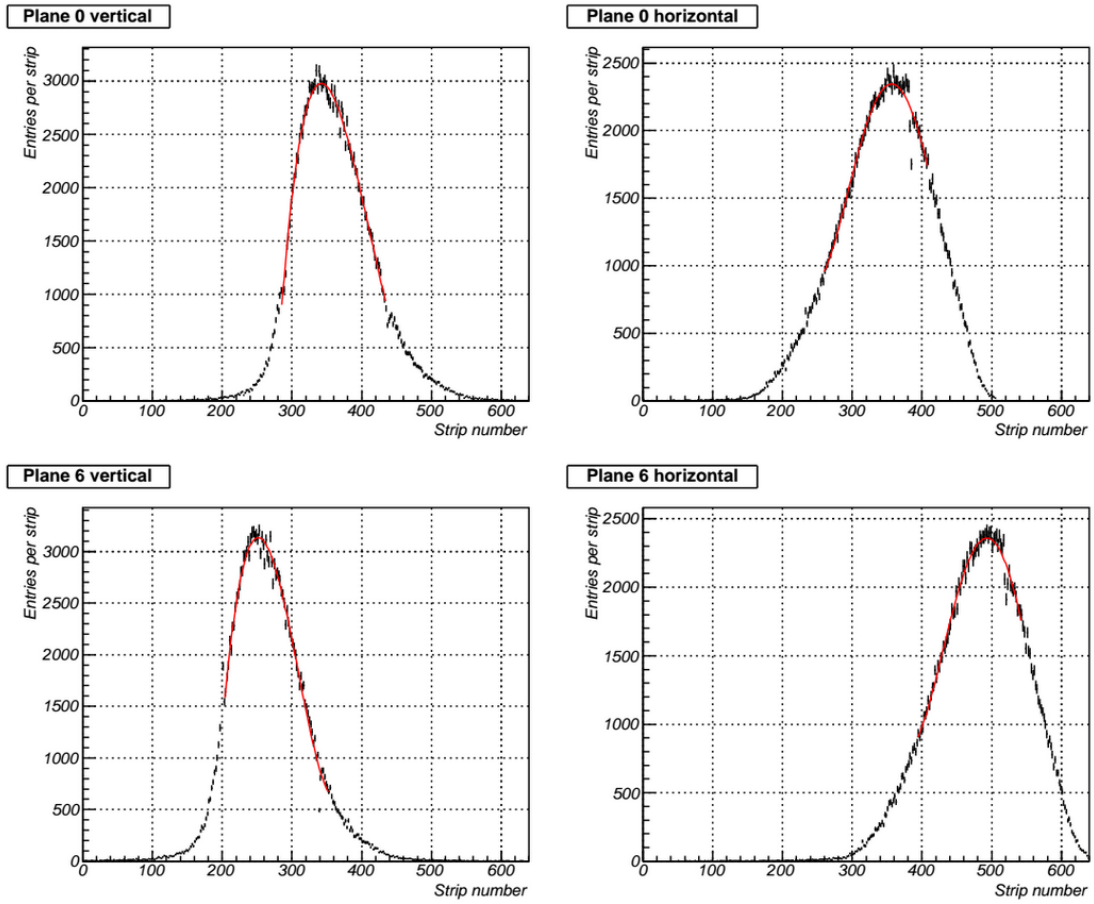

FIG. 6. The locations of hits for two pairs of strips, with one measuring the x-coordinate and the other measuring y in each pair.[5] The peaks are not in the same locations, which indicates that the mechanical alignment is not perfect. This must be accounted for through a software alignment procedure.

so a software alignment procedure is carried out in order to find the correct position of the planes relative to one another. The geometry is then updated with the correct positions and angles of the detectors, and can be used to refit the tracks.

Figure 7 compares a track before and after the software alignment procedure. The track before alignment is indicated with circular points. While there does appear to be a track present, it is not the straight line that is expected of a particle coming from a beam with minimal transverse momentum. After the alignment procedure[6] is completed and the geometry has been updated, the track appears more linear, as shown by the asterisks along the dotted line.

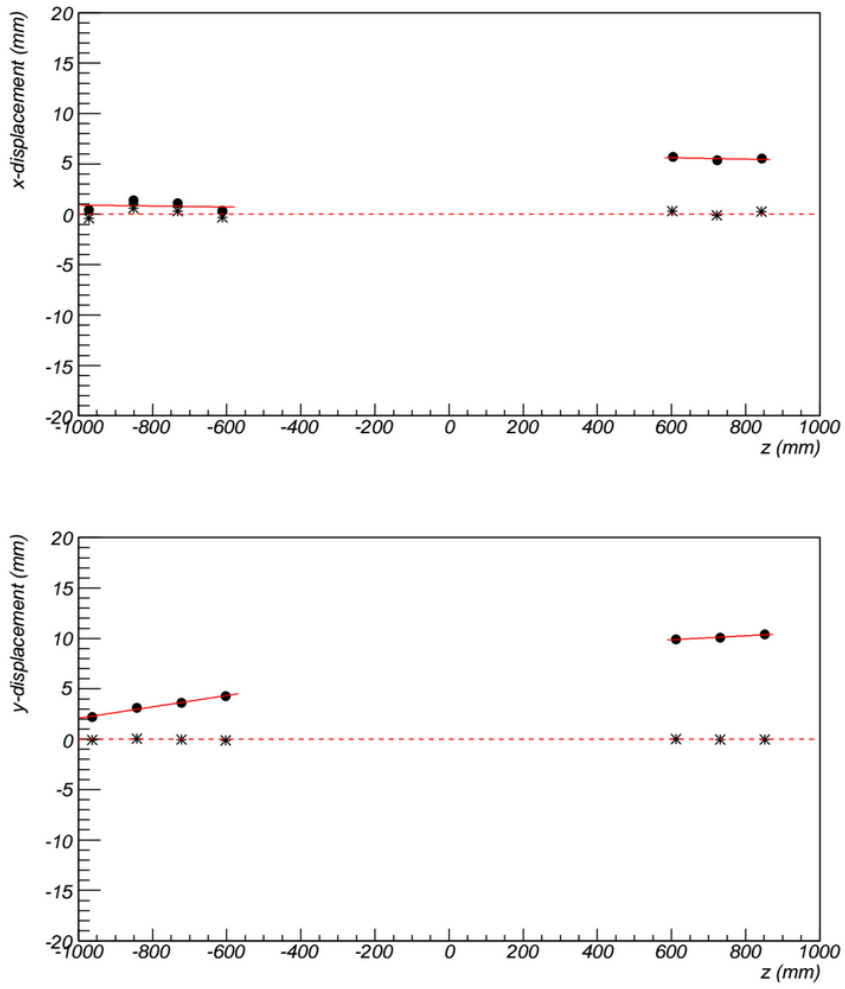

FIG. 7. The circular points show a track, in both the $x-z$ and $y-z$ planes, before alignment. The asterisks along the dotted line show the same track, after proper alignment.[5]

III. NEW FITTING METHOD

A. Kalman filter

A Kalman filter is an algorithm which was first developed by Rudolf E. Kálmán in 1960. It looks at input data over time and recursively predicts the system's state using a least squares method in order to more effectively separate signal and noise.

A Kalman filter was selected in the case of fitting linear particle tracks, due to the fact that the data takes place over time and it is necessary to predict the system's state while accounting for the noise. A notable source of noise in the telescope is the probability of a proton undergoing a multiple scattering event. When a proton passes through a detector, it

often passes through unhindered. Occasionally, it may interact with a nucleus in material along the beamline and can be deflected at some small angle, as shown in Figure 8. Previously, this source of error was not being accounted for in the simple χ^2 minimization fit of the track-fitting procedure, so the Kalman filter was implemented to ensure this error was being handled correctly.

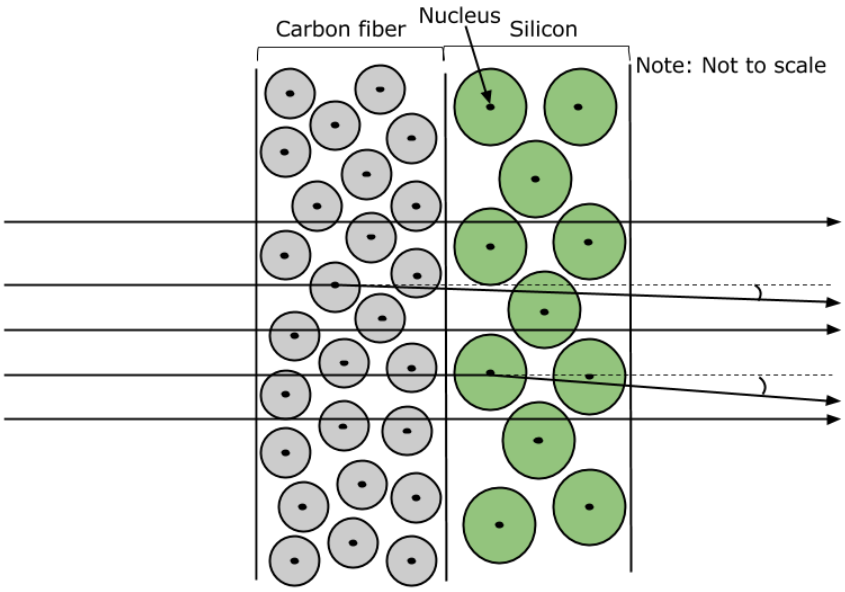

FIG. 8. When a proton passes through a detector, there is some probability of it interacting with a nucleus within the detector. If it does, it may scatter off at some small angle.

B. Implementation

To begin, each track is parametrized using Equations (1) and (2).

$$x(z) = \alpha z + x_0 \tag{1}$$

$$y(z) = \beta z + y_0 \tag{2}$$

The state of the track at the k^{th} plane is given by Equation (3).

$$x_k = \begin{pmatrix} \alpha_k \\ x_{0k} \\ \beta_k \\ y_{0k} \end{pmatrix} \tag{3}$$

The algorithm begins with an initial estimate of the track parameters coming from the simple χ^2 minimization fit. It then runs over all the hits found in a track, using a recursive least squares algorithm to fit the track, while adding one of the covariance matrices found in Equations (4) and (5), where z_k is the z-value of the k^{th} plane and ρ is the probability of scattering, which is the same for all planes.[5] Equation (4) is used in the case of strips, since there is no correlation between x and y, while Equation (5) is used in the case of pixels, since there is indeed correlation between x and y.

$$Q_{k,strips} = \begin{pmatrix} \rho^2 & -z_k\rho^2 & 0 & 0 \\ -z_k\rho^2 & {z_k}^2\rho^2 & 0 & 0 \\ 0 & 0 & \rho^2 & -z_k\rho^2 \\ 0 & 0 & -z_k\rho^2 & {z_k}^2\rho^2 \end{pmatrix} \tag{4}$$

$$Q_{k,pixels} = \begin{pmatrix} \rho^2 & -z_k\rho^2 & \rho^2 & -z_k\rho^2 \\ -z_k\rho^2 & {z_k}^2\rho^2 & -z_k\rho^2 & {z_k}^2\rho^2 \\ \rho^2 & -z_k\rho^2 & \rho^2 & -z_k\rho^2 \\ -z_k\rho^2 & {z_k}^2\rho^2 & -z_k\rho^2 & {z_k}^2\rho^2 \end{pmatrix} \tag{5}$$

1. Scattering probability

The value for ρ is calculated as the width of the distribution of multiple scattering angles, θ, as shown in Equation (6).

$$\rho = \theta/\sqrt{2} \tag{6}$$

The distribution of multiple scattering angles is calculated based on the material thickness, x, the radiation length of the material, X_0, the proton's momentum, p, and its β value. The formula is given by Equation (7).[5]

$$\theta = \frac{(13.6MeV)}{\beta cp}\sqrt{x/X_0}(1 + 0.038\log(x/X_0)) \tag{7}$$

It is assumed that $\beta \approx 1$ and $p = 120$ GeV, since there is little variation between the particles in the beam. The sensors themselves are 300 μm of silicon, and are covered with 300 μm carbon fiber sheets. The relevant values for both silicon and carbon fiber are included in Table I.

	Silicon	Carbon Fiber
x	300 μm	300 μm
X_0	9.36 cm	17.08 cm
x/X_0	3.21×10^{-3}	1.76×10^{-3}
θ	5.02 μrad	3.61 μrad
ρ	3.55 μrad	2.55 μrad

TABLE I. Relevant values for calculating the distribution of multiple scattering angles for silicon and carbon fiber.

Adding the two values of ρ for silicon and carbon fiber in quadrature, a final value of 4.37 μrad is produced for the combined value of ρ.

IV. RESULTS

In order to determine if the Kalman filter works as expected, a sample of 100 000 events was analyzed. Tracks were required to have all hits on all twenty-two planes, so only the most precise tracks were used. About 20 000 tracks passed this cut.

A. Track fitting performance

The success of a fitting method can be measured in a number of different ways, but two main ones are taken into consideration for the telescope.

The first is the distribution of residuals. The residual of a hit is calculated as the difference between the measured location of the hit and the location predicted by the track. Residuals

are calculated in both the x- and y-directions for each detector. The distributions are expected to be symmetric about zero, meaning that the tracks or points do not tend to one side. In addition, the residuals should be distributed in a narrow peak, since small residuals indicate a high precision. So indeed, a narrow peak centered around zero is indicative of a good alignment and good well-fit tracks. An example of a residual distribution can be seen in Figure 9(a). The difference between the measured mean value and zero is less than the error associated with the fit, σ_{fit}, and it appears to be symmetric. It also has a small σ value, which indicates a small resolution on that plane. Overall, these indicators show that the hits on this plane are fit well by the predicted tracks.

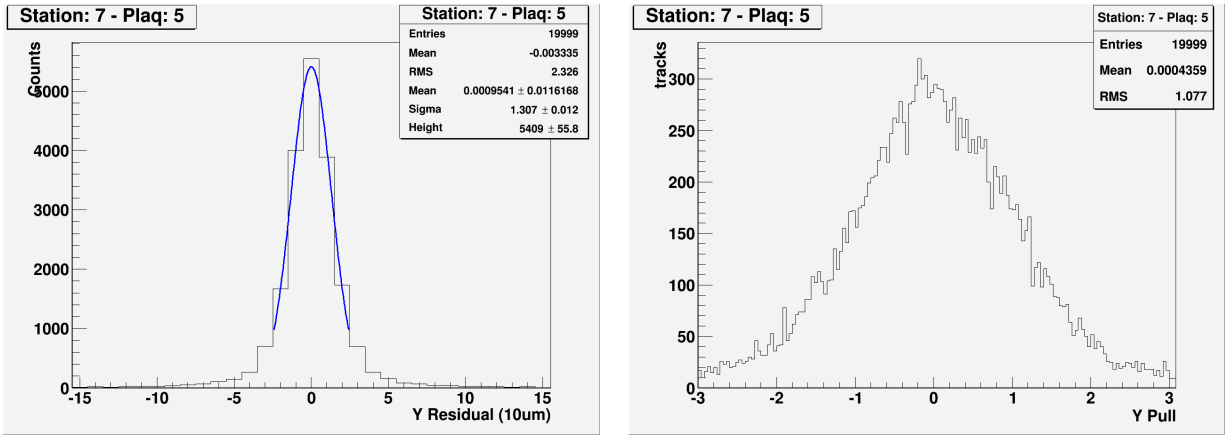

(a) Residual Distribution

(b) Pull Distribution

FIG. 9. *Left:* A distribution of residuals that is narrow and symmetric about zero is indicative of well-fit tracks. *Right:* A distribution of pull values should be symmetric about zero, and the σ or RMS value of the distribution close to one. This suggests that errors are being correctly estimated.

The second is the distribution of pull values. The pull value for a hit is defined as the residual divided by the total error associated with the hit, which includes the measured and projected track errors. The pull is calculated in both the x- and y-directions, corresponding to the x- and y-residuals. These distributions are also expected to be symmetric around zero. They should have σ values near one, indicating that hit errors are being estimated correctly since they are lining up with the residuals being measured. An example of a pull distribution can be seen in Figure 9(b). While not fit with a function, it is clear that it is indeed centered about zero, and is fairly symmetric. In addition, the RMS value, which serves as an estimation of the σ value, is close to one. This shows that the errors on the hits

are being correctly calculated.

A last test of the performance of a track fitting method is the peak value of the χ^2 distribution for all of the tracks. Ideally this value will fall very near to one. If it is larger than one, that indicates that the errors on the tracks are underestimated. Similarly, if it is smaller than one, the errors on the tracks are likely overestimated.

If these conditions on the residuals and pull values are met for most planes of the telescope and the peak χ^2 value for all of the tracks is near one, it is inferred that the fitting method is performing well.

B. Simple fit

Initially, the tracks were fit with the simple χ^2 minimization fit method. Overall, the results are as expected. All the residual distributions are centered around zero, within a maximum of $3.5\sigma_{fit}$. Nine of twenty-two detectors are within $1\sigma_{fit}$ of zero. As shown in Figure 10, the resolution varies between 10 μm, which is a very desirable number, and 20 μm, which is too high for the purposes of the telescope. The strips, which can be seen on the edges of the graph, typically have a notably smaller resolution than the pixels, which are the more constant point towards the middle.

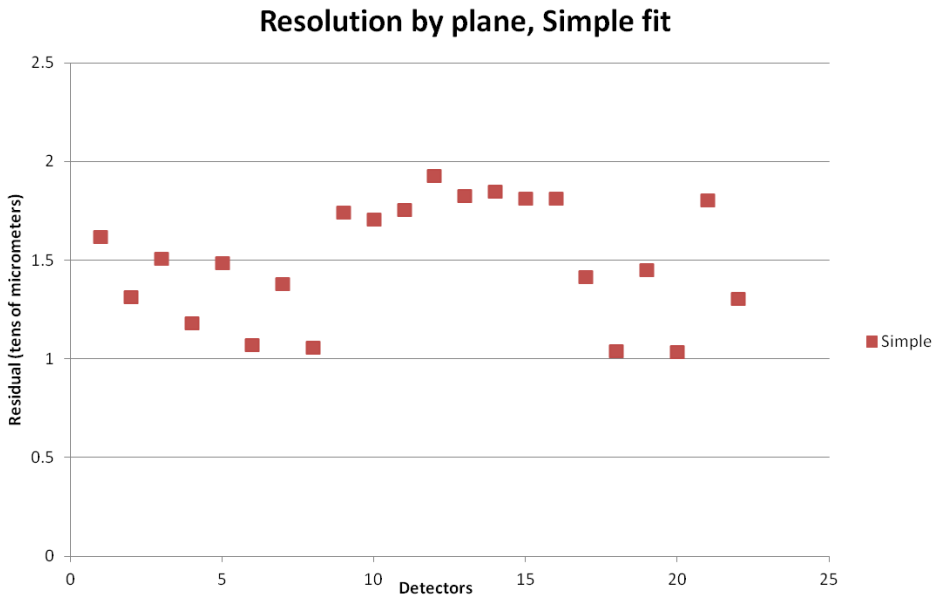

FIG. 10. The values of σ from the residual distributions, or the resolutions, for all planes, using the simple χ^2 minimization fit. All resolutions fall between 10 and 20 μm.

The pull distributions are all centered around one and appear quite symmetric. The RMS values, shown in Figure 11, are usually above one. These values can certainly be improved and moved closer to the desired value of one. The value of χ^2 is 1.16, which indicates that the track errors may be slightly underestimated.

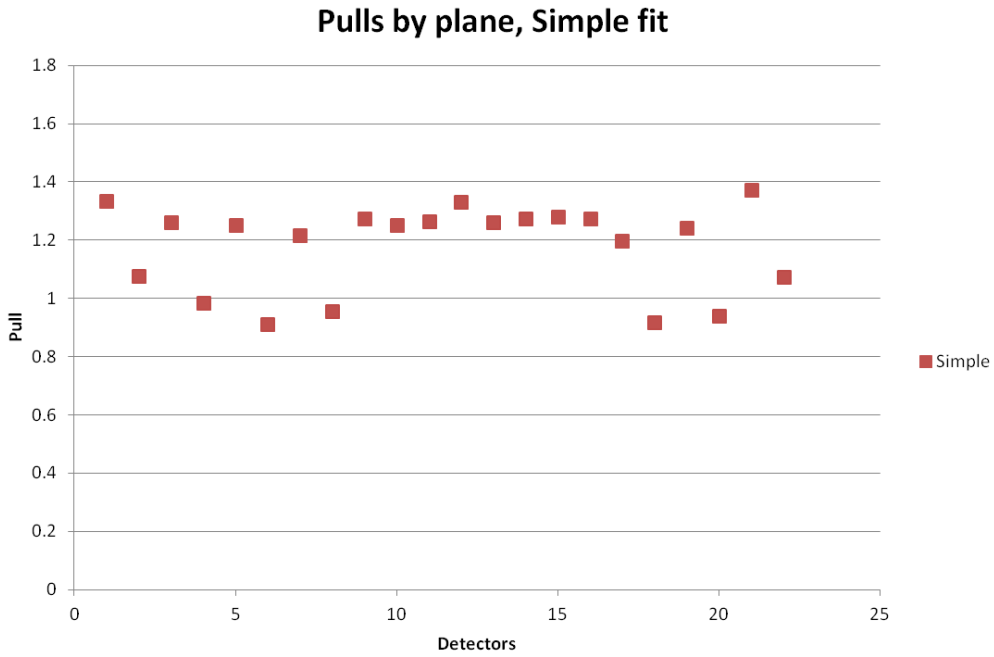

FIG. 11. The RMS values from the pull distributions for all planes, using the simple χ^2 minimization fit. Many values fall above the desired value of one.

C. Kalman filter

1. With scattering

When the Kalman filter is applied, it does not perform as expected. The residuals are still centered around zero, all within $3.5\sigma_{fit}$, and ten are within $1\sigma_{fit}$ of zero. It is important to note that while a fraction of detectors similar to that of the simple fit are within $1\sigma_{fit}$, the σ_{fit} values do increase. As shown in Figure 12, the residuals increase as compared to the simple fit. No detector sees improvement, and the largest increase is around 20 μm.

While the pull distributions are still centered around zero, the RMS values tend to drop compared to the simple fit, as shown in Figure 13. Not all of this is undesired, since fifteen of twenty-two detectors have their pull values move closer to one. In addition, the value of

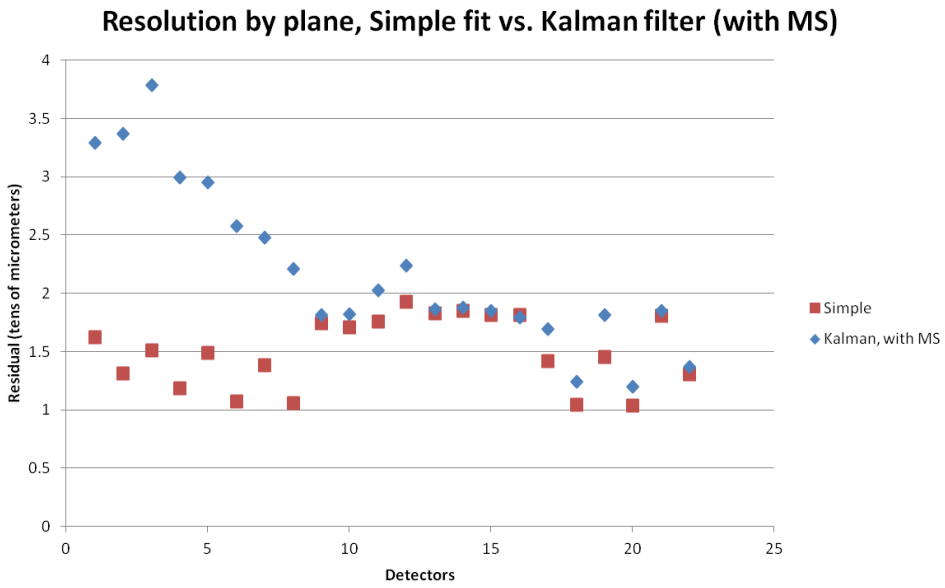

FIG. 12. The resolutions for all planes, using the Kalman filter fit. The resolution of every detector increases over the simple fit values.

χ^2 decreases to 0.95, which is an improvement. These two points indicate that the Kalman filter may be treating errors more correctly than the simple fit, due to the fact that it is accounting for the probability of scattering. Still, this cannot make up for such large resolutions, and the method must be changed or another solution found.

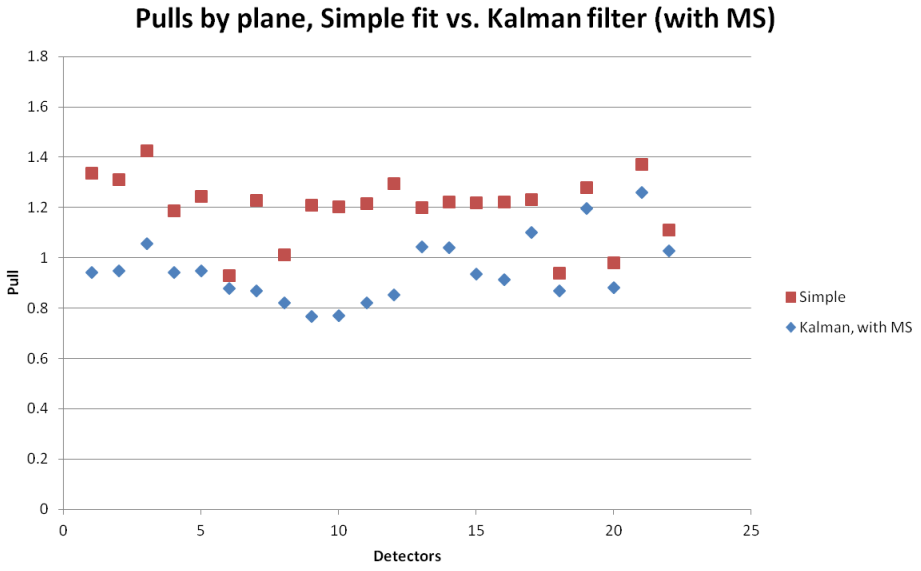

FIG. 13. After the Kalman filter, the RMS values from the pull distributions for fifteen of twenty-two detectors move closer to the desired value of one, as compared to the simple fit values.

2. *Without scattering*

Results improve significantly if the structure of the Kalman filter is retained and the scattering probability reduced to zero. The distributions of residuals are still centered around zero. There are three outliers that are 3.5 - $7\sigma_{fit}$ away from zero, though it is important to note that σ_{fit} tends to shrink. Despite that, eleven of twenty-two are still within $1\sigma_{fit}$ of zero. In addition, all distributions remain symmetric. Comparing the results of the partial Kalman filter to those of the simple fit, the resolution is improved for nineteen out of twenty-two detectors. This can be seen in Figure 14.

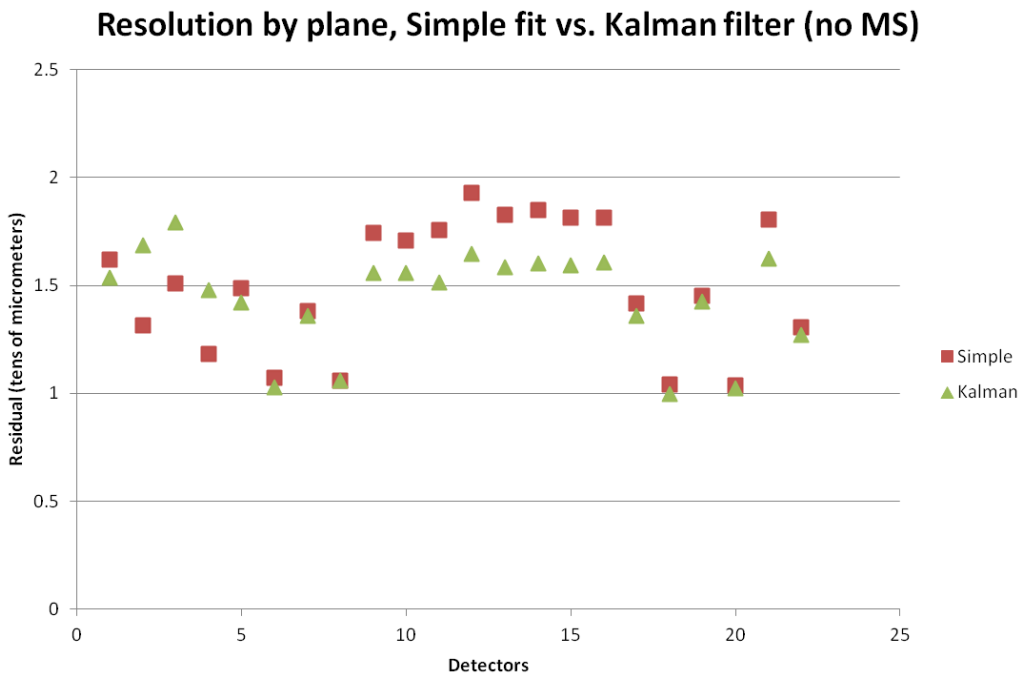

FIG. 14. The resolutions for all planes, using the Kalman filter fit assuming no multiple scattering. Improvement, most notably in the pixels, can be seen over the simple fit in nineteen of twenty-two detectors.

The pull values also improve for a majority of the detectors. All of the pixel detectors as well as six of the fourteen strips see a decrease, as shown in Figure 15. The χ^2 value increases to 1.21, which is a small margin above the simple fit value. So while the pulls are improved, there is evidence that the errors are still being underestimated.

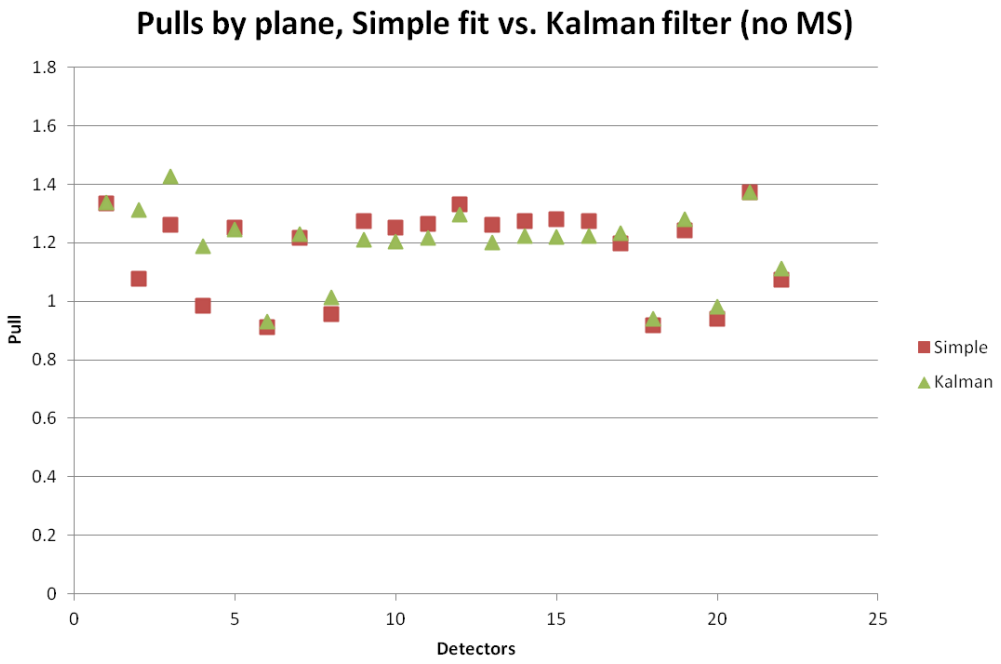

FIG. 15. The RMS values from the pull distributions for all planes, using the Kalman filter fit, assuming no multiple scattering. The values for fourteen of twenty-two detectors move closer to the desired value of one as compared to the simple fit values.

V. CONCLUSIONS

The main goal of the silicon tracking telescope is to provide users with high precision tracking information. For this reason, more strip detectors will be incorporated into the telescope, and the pixels will be removed. The narrower dimension of the strips will provide users with a better resolution, and the larger coverage area will make the telescope able to test larger devices.

There is still much work to be done before the full Kalman filter, including scattering probability, can be used. There are a number of potential improvements, as addressed below, to be made, all of which should be addressed before the full filter is used in a formal analysis.

The large residuals at the beginning of the telescope after the Kalman filter are not surprising. Since multiple scattering is occurring along the full length of the telescope, and the location of the particle is known at the end, the is more uncertainty assigned to where it is at the beginning. This larger error corresponds to larger residuals, as seen in the data. Typically, when a Kalman filter is applied, a smoothing algorithm, using information from neighboring planes to locally smooth the track, is used to further adjust the fitted tracks,

reducing this effect. In this implementation, no such algorithm was applied, so an obvious next step is to build this step into the track fitting procedure.

In addition, the multiple scattering probability could be estimated incorrectly. Upon closer scrutiny, the mathematics seems sound. While this is not thought to be a contributing factor, it may require further investigation.

After examining how error is assigned to individual hits, it is believed that this error is not being calculated correctly. Incorrect error on individual points can lead to large resolutions and small pulls, as we observe in the data. If this calculation is corrected, there would likely be improvement in residuals, as well as pulls.

The measured positions of clusters may also not be calculated precisely due to the fact that the strip detectors have not yet been calibrated. The values for clusters of size two depend upon the uncalibrated charge value and thus might not be precise. Since all strip planes are tilted along the short dimension of the x-measuring planes, those planes have a notably larger number of clusters of size two as compared to those measuring the y-coordinate, meaning that the positions of hits on strips measuring the x-positions are less accurate. This would cause a difference between the x- and y-residuals for strip detectors, which is indeed seen in the data.

While clearly the Kalman filter is not fully functional when the probability of scattering is introduced, the data shows there is nothing wrong with the structure of the filter itself. In fact, assuming no multiple scattering, it is an improvement to the simple χ^2 minimization fit method. This is illustrated by improved residual and pull values for nearly all detectors. Thus, the Kalman filter will be the preferred fitting method in future analyses.

ACKNOWLEDGMENTS

Many thanks to my mentor, Dr. Lorenzo Uplegger, for his unceasing help and patience; to the Electrical Systems Engineering Department and the Scientific Computing Division for the use of their facilities and resources; to Fermilab and its staff, for hosting me as a summer intern and providing a wealth of opportunities for the interested student; and to the Department of Energy, for funding my research.

REFERENCES

[1]S. Kwan, C. Lei, D. Menasce, L. Moroni, J. Ngadiuba, A. Prosser, R. Rivera, S. Terzo, M. Turqueti, and L. Uplegger, "The CMS pixel tracking telescope at the Fermilab Test Beam Facility," (2013).

[2]M. Demarteau, R. Demina, S. Korjenevski, R. McCarthy, F. Lehner, R. Smith, R. Lipton, and H. Mao, "Characteristics of the layer 1 silicon sensors the run IIb silicon detector," (2003), D0-note 4309.

[3]K. Kahle and L. Rossi, "Designs on higher luminosity," CERN Courier (2012).

[4]D. Menasce, S. Terzo, and L. Moroni, "Monicelli [Computer Software]," (2011), Milano, Italy: I.N.F.N Milan-Bicocca.

[5]M. Jones, "Strip telescope alignment," (2014).

[6]L. Moroni, "Alignment algorithm for the pixel telescope at MTEST," (2011).